RSC Advances

ROYAL SOCIETY OF CHEMISTRY

www.rsc.org/advances

RSC Advances

ARTICLE

Characteristics of Ultrasonication Assisted Assembly of Gold Nanoparticles in Hydrazine Reduced Graphene Oxide

Kashyap Dave[a], Kyung Hee Park[b], Marshal Dhayal[a†]

[a] Clinical Research Facility, Medical Biotechnology Complex, CSIR-Centre for Cellular and Molecular Biology, Hyderabad 500007, India.

[b] Department of Dental Materials and Medical Research Center for Biomineralization Disorders, School of Dentistry, Chonnam National University, Gwangju 61186, Korea.

[†]Corresponding Author (E-mail: marshal@ccmb.res.in, Tel: +91-(0)-271-92500 Fax: +91-(0)-40-271-60591)

Abstract

Here we report a new ultrasonication assisted method for increased diffusion of gold salt in hydrazine reduced graphene oxide (hrGO) sheets. Gold nanoparticles (AuNP) were formed through *in-situ* reduction of diffused gold chloride within the hrGO sheets by sodium borohydride. Transmission electron microscopic (TEM) analysis confirmed uniform distribution of ~5-10 nm AuNP in hrGO sheets. Raman spectra of hrGO-AuNP showed an increase in the ratio of D- band to G- band intensity as well as the absence of 2D band. This confirmed distortion of multilayer assembly into much thin layers by the process of AuNP nucleation in the composite material. X-ray diffraction (XRD) spectra of hrGO-AuNP confirmed the presence of

crystallite carbonic materials and AuNP by observing strong diffraction peaks of Au (111), Au (200), Au (220) and Au (311). UV-visible spectra of oxide hrGO-AuNP showed a spectral shift of 21 nm in reduced graphene oxide which confirmed the binding of AuNP with hrGO. X-ray photo electron spectroscopy (XPS) analysis revealed 13.4, 69.3, 13 and 2.3 % mass proportions for gold, carbon, oxygen and nitrogen, respectively in hrGo-AuNP. XPS analysis also showed an increase in sp^3 carbon as compare to sp^2 carbon in C1s after gold nucleation in hrGO. I-V response of hrGO remained unaffected by the nucleation of AuNP in hrGO composite material. This method may be useful to address the challenges associated with incorporation of metals into reduced graphene oxide without chemical functionalization of inert surfaces.

1. Introduction:

The discovery of graphene, a sp^2 hybridized two-dimensional crystalline carbonic material [1], has increased the interest of using this material in several industrial applications due to its unique properties in electron transportation [2-3], thermal conductivity [4], mechanical stiffness [5] and optics [6]. In the last few years, choice for a range of surface modifications of graphene oxide /reduced graphene oxide make it more suitable for preparing a range of composite materials [7-9]. Several studies have been carried out to understand the properties of synthesized composite materials of graphene by incorporating metal nanoparticles, polymer and active molecules [10-13].

Graphene based composite materials have already been used for transistors [3,14,15], antibacterial material coating [16], batteries and photovoltaic cells [17-25], and catalyst [26-31]. Few recent studies have showed potential applications of graphene sheets-sulfer / carbon composites in preparation of lithium sulfer battery [18] and phosphorene-graphene oxide composites as anode in sodium-ion battery [15]. Efficiency and stability of organic photovoltaic cell has been improved by making an additional layer of lithium-neutralized graphene oxide

introduced between the photoactive solar cells and electron transport layers [20]. In a recent study by Chen et. al. [32] enhancement in the short-circuit photocurrent density in screen printed solar cells have been described by using doped wrinkle graphene sheets. Photo conversion efficiency of organic photovoltaic device had an increased response by incorporation of gold nanoparticles in graphene oxide thin film [33]. Excellent micro wave absorption properties of graphene composite materials have been reported with the addition of oxide/iron/polyaniline [34]. Various other properties of graphene composite materials have been utilized in several applications such as: FRET based biosensor to detect the DNA with high sensitivity and specificity have been fabricated by using graphene oxide-NaYF4:Yb,Er composites [35]. Pollutes in river water have been detected by using reduced graphene oxide- MnO_2/Ag composite materials [36]. The use of graphene gold composite as a catalytic for degradation of 4-nitrophenol dye molecules has been also evaluated [37].

A study by Muszynski et. al. [38], synthesis of graphene-gold composites have been reported and have showed that the functionalization of graphene with octadecylamine is necessary before addition of $HAuCl_4$ while reducing by sodium borohydride. This study demonstrated that graphene oxide without surface modification have poor ability for preparing gold composites. Recently Jungemann et. al. [39] reported a step by step programmable method for gold nanoparticle incorporation into oligonucleotides functionalized graphene. A controlled concentration of gold-graphene composite can be achieved in above described method; however, again it requires functionalization of graphene sheets for assembly of gold nanoparticles on graphene. This finding suggests that the nucleation of gold nanoparticles can not be started in reduced graphene oxide in the absence of oxygen functionality at the surface of graphene oxide. Recent progress made in the field of graphene hybrid architectures with a focus on the synthesis

of graphene-carbon nanotube, graphene-semiconductor nanomaterial, and graphene-metal nanomaterial hybrids have been well reviewed by Badhulika et. al. [40].

Here we describe a simple approach for the synthesis of hrGO-AuNP composite materials using ultrasonication assisted assembly of *in-situ* gold nanoparticle formation within reduced graphene oxide. This can be achieved without surface modification or functionalization of reduced graphene oxide with organic molecules. The process has been optimiz for the synthesis of hrGO-AuNP composite and optimum concentration obtained to achieve a better distribution of gold nanoparticles in hrGO. Changes in the surface chemistry of reduced graphene oxide before and after gold nucleation were characterized by XPS. TEM was used to quantify the distribution of gold particles in hydrazine reduced graphene oxide sheets.

2. Materials and Methods:

2.1. Materials:

Sulphuric acid (H_2SO_4) and hydrochloric acid (HCl) were obtained from RANKEM. Sodium nitrate ($NaNO_3$), methanol, potassium permanganate ($KMnO_4$) and hydrogen peroxide (H_2O_2) were purchased from SRL, MERCK, and SDFCL. Sodium borohydride ($NaBH_4$), hydrazine hydrate and Gold chloride ($HAuCl_4$) were purchased from Sigma Aldrich. Graphite flakes were obtained from CDH. Milli-Q water (18 ohm) was used as a solvent in all the experiments. Other chemicals used in the experiments were analytical grade and purchased from local suppliers.

***2.2 Synthesis of Hydrazine Reduced* Graphene Oxide (GO)** Modified Hummer's method used for the synthesis of GO as described in previous studies [41, 42]. During synthesis, H_2SO_4 was added in the mixture of graphite flakes and $NaNO_3$, stirrered at 0-4°C to obtain homogeneous solution. $KMnO_4$ was added gradually to the homogeneous solution of graphite as described elsewhere [43].

200 mg of vacuum dried and thoroughly washed synthesized GO was dispersed in water by sonication for 180 mins to prepare 1 mg/ml solution. In above solution, 2ml of 64.2 mM hydrazine hydrate was added and the reaction was carried out at 95^{o}C for 24 h [44]. The precipitate was filtered and washed by methanol, HCl and water. Material was dried at room temperature in vacuum for 2 days.

2.3 Synthesis of hrGO-AuNPs composites

To synthesize composite material, 50 mg hrGO was mixed in 198 mL water. A homogenous solution of hrGO was obtained after 120 mins of sonication in which 2 ml of 1 % (w/v) $HAuCl_4$ was added. The mixture was further sonicated for 30 mins followed by the addition of 1.36 mM $NaBH_4$. Finally the solution was incubated for 30 mins to complete reduction process. A schematic representation of experimental steps for the synthesis of hrGO-AuNP has depicted in Figure 1. Optical image of the product in water suspension was taken at each stage and have shown in the schematic representation. We hypothesized that the gold chloride solution was diffused inside the reduced graphene oxide sheet during sonication process for 30 mins. Therefore addition of sodium borohydride initiated in-situ formation of AuNP at the diffused site inside the reduced graphene oxide sheets.

To obtained hrGO-AuNP composites, we removed unbound gold nanoparticles from the suspension by filtration and washed three times separately by methanol, 1 M HCl and water. Finally the filtrate was dried in a vacuum system for three days and powers form of hrGO-AuNP was obtained. This power was used for further characterization to understand the characteristics of hrGO-AuNP.

2.5 Characterization

The crystal structures of graphite and synthesized carbonic materials were characterized by various techniques. Raman spectra were obtained by RENISHAW System at 633 nm laser. Absorption spectra were measured by UV-2600 SHIMADZU Spectrophotometer between 200-700 nm. The crystallite structure of **GO**, **hrGO** and **hrGO-AuNP** was characterized from XRD pattern using XRD-6000 (Japan) X-ray diffractometer in the diffraction angle range 5–80° with Cu-Kα radiation (λ= 1.54060 Å). X-ray photoelectron spectra of hrGO and hrGO-AuNP were obtained on a MultiLab200 with standard MgKα radiation to quantify elemental composition and surface states of carbonic materials. All spectra were taken at a working pressure of 10^{-9} mbar. Wide scan XPS survey was used for elemental proportion quantification and high-resolution spectra of C1s was used for characterization of surface functionalities. The different surface states were obtained in the high resolution C1s spectra by specifying line shape, relative sensitivity factor, peak position, full width at half maxima, and area constraints. Sonication of the material was carried out at 21 % of amplitude in SONICES vibracell. TEM images were obtained at 120KV acceleration voltage using JEOL (Japan) transmission electron microscope.

3. Results and Discussion

Figure 2 shows UV-Vis spectra of **GO, hrGO** and **hrGO-AuNP** colloidal suspension in water. UV-vis spectra of GO showed strong absorption peak at 235 nm due to π-π^* interaction of C=C. Additionally a solder peak at 305 nm was also observed due to π-n* interaction between oxygen and carbon representing C=O bond in GO. Spectra peak at 270 nm correspond to π-π^* interaction of C=C in reduced graphene oxide. Solder peak at 305 nm in UV-vis spectra of hrGO was disappeared which confirms the removal of oxygen functionality due to reduction of GO in hrGO. UV-vis spectra of hrGO-AuNP colloidal suspension showed a strong absorption at 249.5 nm which corresponds to sp^2 carbonic bonding of reduced graphene oxide. Absorption peak at 249.5 nm which corresponds to π-π^* interaction of sp^2 carbonic bonding of C=C in hrGO-AuNP.

A blue shift of 21 nm in the spectra was observed as compared to hrGO due to binding of AuNP with hrGO.

Raman spectra of pristine graphite and synthesized **GO**, **hrGO** and **hrGO-AuNP** are shown in **Figure 3**. Graphite Raman spectra had strong peaks at 1583 cm^{-1} and 2666 cm^{-1} which were corresponds to the G band and 2D band, respectively [42]. A small peak corresponds to D band at 1341 cm^{-1} was also observed. Raman spectra of GO showed a wide peak at 1596 cm^{-1} due to stretching of the C-C bond. Peak intensity ratio for D-band (I_D) and G-band (I_G) peaks were 0.8 and 1.01 for graphite and **GO**, respectively. Relative peak intensity of D-band at 1341 cm^{-1} increased as compared to G-band at 1583 cm^{-1} in **GO** in relation with graphite. Thus, the increased intensity of the peak at 1349 cm^{-1} represented an increased in the levels of disorder by the oxidation of graphite in GO. Our observations are consistent with previously reported findings [44,45]. Peak at 2666 cm^{-1} in **GO** Raman spectra was not observed due to conversion of graphite into GO.

hrGO Raman spectra showed D-band and G-band peaks at 1329 cm^{-1} and 1586 cm^{-1}, respectively. D-band intensity was relatively high as compared to the G-band. The peak intensity ratio of I_D/I_G for **hrGO** was 1.04. Raman spectra of **hrGO-AuNP** had a similar pattern to **hrGO** with increased I_D/I_G (~1.12) ratio. Raman spectra of **GO**, **hrGO** and **hrGO-AuNP** at different laser power exposures at 633 nm was measured and results are shown in **SFig. 1**. **GO** Raman spectra showed a significant decrease in single to noise ratio at higher laser powers. There were no significant changes in the signal to noise ratio in the Raman spectra of **hrGO** and **hrGO-AuNP** with an increase in laser power.

XRD spectra of synthesized **GO**, **hrGO** and **hrGO-AuNP** are shown in **Figure 4**. XRD spectra had a sharp peak at $2\vartheta \sim 10.1^{o}$ which corresponds to the reflection from the (002) plane [46]. A peak at $2\vartheta \sim 42.8^{o}$ may correspond to the turbostratic band of disordered carbon materials. XRD

spectra of **hrGO** had a wide peak around ~ 23° of value 2ϑ. Peak at 2ϑ ~ 10.1° was completely disappeared and peak at 2ϑ ~ 42.8° was widened. The broad diffraction peak of **hrGO** indicates poor ordering of the sheets along the stacking direction. XRD spectra of **hrGO-AuNP** composite showed both peaks at 2ϑ ~ 23° and ~ 42.8° corresponding to crystallite carbonic materials. The presence of gold showed strong diffraction at 2ϑ ~ 38.4°, 44.6°, 64.2° and 77.5° which corresponds to Au (111), (200), (220) and (311) plans.

TEM images of **hrGO-AuNP** composite material are shown in **Figure 5**. Well dispersed AuNP were present in the sheets of hrGO. Careful analysis of **hrGO-AuNP** TEM image indicated folding of reduced graphene oxide sheets and deep penetration of **AuNP**. The average particle size of AuNP in the hrGO sheets was between 5 to 10 nm, however at few locations large size of partial distribution was seen. This may be due to multiple folding of reduced graphene oxide sheets. Both TEM and XRD analysis confirms the presence of gold nanoparticles in the synthesized hrGO-AuNP composite material.

XPS analysis was used for estimation of the percentage (%) proportion of gold incorporated in composite materials. Wide scan XPS spectra of synthesized **GO**, **hrGO** and **hrGO-AuNP** was obtained and is shown in **Figure 6**. Carbon and oxygen % mass ratio in synthesized **GO** was 54.4% and 45.3 %, respectively. Small amount of nitrogen mass proportion (0.3%) was also observed which could be due to adsorption of nitrogen from the environment. Spectra of **hrGO** showed significant decrease (45.3 to 14.6%) in the percentage proportion of oxygen and increased % proportion of carbon (54.4 to 81.5%). In addition very significant amount of nitrogen (3.9 % mass proportion) was also observed. The increased amount of nitrogen could be associated with the residue of N_2H_2 used for reduction of **GO** which probably due to the presence of impurities even after several time washes and vacuum drying. XPS wide scan of **hrGO-AuNP**

composite showed 13.4 % mass proportion as gold and 69.3, 13 and 2.3 % mass proportions of carbon, oxygen and nitrogen, respectively.

High resolution C1s XPS analysis of GO was carried out and results are shown in **Figure 7A**. The higher resolution C1s XPS spectra of GO was fitted with six peaks of different carbon environments as: hydrocarbon (C=C), (C-C/C-H), (C-OX), (C=O/O-C-O), (C(=O)OX) and satellite peak due to π-π interactions. XPS spectra before and after nucleation of gold with hrGO obtained and results are shown in **Figure 7B&C**. The peak fitting for surface state quantification from C1s was done as described in previous study [47]. C1s peak mainly fitted as hydrocarbon (CC), hydroxyl/carbonyl (COX), C=O/O-C-O and carboxylic functionality peaks [48,49]. Separately two peaks of hydrocarbons as C1s (C=C, sp^2 carbon) and C1s (C-C, sp^3 carbon) fitted for a better representation of XPS observations [43]. Shake-up peak associated with carbon in aromatic ring was identified at the tail of the spectra towards higher binding energy and it was separately assigned during the peak fitting [50].

The higher resolution C1s XPS spectra of N_2H_4 reduced **GO** composite was fitted as: hydrocarbon (C=C) at 284.2 eV, (C-C/C-H) at 285.7 eV, (C-OX) at 287.1 eV, (C=O/O-C-O) at 288.6 eV, (C(=O)OX) at 290.3 eV and shake-up peak at 292.8 eV. The position of each peak associated with C-OX, (C=O/O-C-O) and (C(=O)OX) were fixed by assigning 1.5 ± 0.3 eV shift in the binding energy, respectively [51]. Previously Chu et. al. [48] had characterized amorphous and nanocrystalline carbon films and observed about ~1.7 eV difference in the binding energy associated with C1s (sp^2) and C1s (Sp^3) peak of carbon. During peak fitting we observed about ~1.5±0.3 eV difference in the binding energy for C1s (sp^2) and C1s (sp^3). The percentage proportion of different carbon environments in C1s was 64.8, 17.2, 8.4, 3.2 and 5.6 which corresponds to the C=C, C-C/C-H, C-OX, C=O/O-C-O and C(=O)OX respectively.

The higher resolution C1s XPS spectra of **hrGO-AuNP** composite (after nucleation of gold in **hrGO**) was fitted with six peaks of different carbon environments as: hydrocarbon (C=C) 284.2 eV, (C-C/C-H) at 285.7 eV, (C-OX) at 287.1 eV, (C=O/O-C-O) at 288.6 eV, (C(=O)OX) at 290.2 eV and satellite peak at 292.8 eV due to π-π interactions. The percentage proportion of different carbon environments in C1s was 61.6, 19, 9.9, 3.1 and 5.8 which corresponds to the C=C, C-C/C-H, C-OX, C=O/O-C-O and C(=O)OX, respectively. An increase in C1s as C-C (sp^3 carbon) was observed as compared to C=C (sp^2 carbon) after gold nucleation in **hrGO**. Table 1 shows relative variation of different functionalities in synthesized GO, hrGO and hrGO-AuNP.

The effect of the nucleation of gold in reduced graphene oxide on electronic properties and I-V characteristics of hrGO and hrGO-AuNP were investigated as shown in Figure 8. The linear response of the I-V corresponds to metallic properties of the synthesized hrGO and hrGO-AuNP. Using the slop of the curves, electrical sheet resistance (R_s) of the hrGO and hrGO-AuNP sheets was estimated and found to be 2.7×10^5 Ω/sq and 3×10^5 Ω/sq respectively. We have not observed current conducting in the GO, therefore as per the instrument limitation of current measurement; the R_s of GO was estimated to be in the order of 10^{11} Ω/sq or higher. The nucleation of gold in reduced graphene oxide had no significant influence in I-V response of composite material. The release of AuNP from the **hrGO-AuNP** composite material was assessed at various sonication time by observing UV-vis spectra at 0, 10, 20 and 30 mins of sonication time (supporting information, **SFig2**). Gold SPR peak in the composite material was absent at zero time point of the sonication [38]. However, at later time points of the sonication showed an increase in the peak intensity of both reduced graphene oxide and SPR peak of AuNP. This increase may be due to better dispersion of reduced graphene oxide at higher sonication time. Previously large interest in exploring Pt-free counter electrodes (CE) for dye sensitize solar cells (DSSC) has been explored and graphene has been demonstrated to be a promising CE material for DSSCs due to

its excellent conductivity and high electrocatalytic activity [52]. In the future, we plan to use hrGO-AuNP for solar cell application.

Conclusions

Ultrasonication assisted method for increased diffusion of gold salt in **hrGO** sheets was developed and in-site reduction of diffused gold chloride in graphene sheets was achieved with sodium borohydride. The TEM analysis confirmed uniform distribution of ~10nm AuNP in **hrGO** sheets. Functional and structures analysis of **hrGO** before and after gold nucleation showed separation of multilayer assembly of **hrGO** into single layers by the nucleation process of gold nanoparticles in the composite material. The relative proportion of gold in the **hrGO-AuNP** composite material was 13.4 % mass proportion. Liner I-V response was observed for **hrGO** and **hrGO-AuNP** composite material. This method may have advantages in the future for incorporation of metals in reduce graphene without further chemical functionalization.

Acknowledgements

This work was supported by network project (NanoSHE) of Council for Scientific and Industrial Research (CSIR), Ministry of Science and Technology, Govt. of India. #KD is a Project Student at CCMB from Centre for Converging Technologies, University of Rajasthan, Jaipur 302004, India. We are thankful to Mr. Harikrishan, CCMB TEM facility for obtaining TEM images of composite material.

Notes and references

1 K. S. Novoselov, A. K. Geim, S. V. Morozov, D. Jiang, Y. Zhang, S. V. Dubonos, I. V. Grigorieva and A. A. Firsov, *Science*, 2004, **306**, 666–669.

2 Y. Zhang, Y. W. Tan, H. Stormer and P. Kim, *Nature*, 2005, **438**, 201- 204.

3 K. S. Novoselov, A. K. Geim, S. V. Morozov, D. Jiang, M. I. Katsnelson, I. V. Grigorieva, S. V. Dubonos and A. A. Firsov, *Nature*, 2005, **438**, 197-200.

4 J. Baringhaus, M. Ruan, F. Edler, Tejeda, M. Sicot, A. T. Ibrahimi, A.P. Li, Z. Jiang, E. H. Conrad, C. Berger, C. Tegenkamp and W. A. Heer, *Nature*, 2014, **506(7488),** 349-54.

5 I. A. Ovidco, *Rev. Adv. Mater. Sci.*, 2013, **34**, 1-11.

6 L. A. Falkovsky, *J. Phys: Conf. Ser.*, 2008, **129,** 012004.

7 Y. Wang, S. Zhang, D. Du, Y. Shao, Z. Li, J. Wang, M. H. Engelhard, J. Li and Y. Lin, *J. Mater. Chem.*, 2011**, 21**, 5319-5325.

8 X. J. Lv, W. F. Fu, H. X. Chang, H. Zhang, J. S. Cheng, G. J. Zhang, Y. Song, C. Y. Hu and J. H. Li*, J. Mater. Chem.,* 2012**, 22**, 1539-1546.

9 C. Li, Y. Yang, B. Zhang, G. Chen, Z. Wang and G. Li, *Part. Syst. Charact.*, 2014, **31**, 201-208.

10 Z. S. Qian, X. Y. Shan, L. J. Chai, J. R. Chen and H. Feng, *Biosens. Bioelectron.*, 2015**, 68,** 225-231.

11 L. Wang, J. Zhu, H. Yang, F. Wang, Y. Qin, T. Zhao and P. Zhang, *J. Alloys Compd*., 2015, **634**, 232-238.

12 M. Gkikas, *Curr. Org. Chem*., 2015, **19**, 1773-1790.

13 M. Gkikasa, G. V. Theodosopoulosa, B. P. Dasb, M. Tsianoub, H. Iatroua, G. Sakellarioua, *Eur. Polym. J.,* 2014, **60**, 106-113.

14 F. Schwierz, *Nat. Nanotechnol.*, 2010, **5**, 487–496.

15 J. Sun, H. W.Lee, M. Pasta, H. Yuan, G. Zheng, Y. Sun, Y. Li and Y. Cui, Nature Nanotechnology, 2015,**10**, 980–985.

16 A. Janković, S. Eraković, M. V. Sekulić, V. M. Stanković, S. J. Park and K. Y. Rhee, *Progress in Organic Coatings*, 2015, **83,** 1-10.

17 J. Hassoun, F. Bonaccorso, M. Agostini, M. Angelucci, M. Grazia Betti, R. Cingolani, M. Gemmi, C.Mariani, S. Panero, V. Pellegrini, and B. Scrosati, *Nano Lett.*, 2014, **14**, 4901-4906.

18 Chen, T. Zhao, T. Tian, S. Cao, P. R. Coxon, K. Xi, D. F. Jimenez, R. V. Kumar and A.K. Cheetham, *APL Mater.,*2014, **2**, 124109.

19. E. Stratakis, K. Savva, D. Konios, C. Petridis, and E. Kymakis, *Nanoscale*, 2014, **6**, 6925-6931.

20. G. Kakavelakis, D. Konios, E. Stratakis, and E. Kymakis, *Chem. Mater.*, 2014, **26**, 5988–5993.

21 D. Konios, C. Petridis, G. Kakavelakis, M. Sygletou, K. Savva, E. Stratakis, and E. Kymakis, *Adv. Funct. Mater.*, 2015, 25, 15, 2213-2221.

22 D. Yang, L. Zhou, L. Chen, B. Zhao, J. Zhang, *Chem. Commun*., 2012, **48,** 8078–8080.

23 N. Balis, D. Konios, E. Stratakis, and E. Kymakis, *ChemNanoMat*, 2015, **5**, 346-352.

24. M. M. Stylianakis, D. Konios, G. Kakavelakis, G. Charalambidis, E. Stratakis, A. G. Coutsolelos, E. Kymakis, and S. H. Anastasiadis, *Nanoscale,* 2015, **7**, 17827-17835.

25. J. Liu, Y. Xue, Y. Gao, D. Yu, M. Durstock, L. Dai, *Adv. Mater*. 2012, **24**, 2228–2233.

26 R. Raccichini, A. Varzi, S. Passerini and B. Scrosati, *Nat.* Mater., 2015, **14,** 271-279.

27 V. Tozzini and V. Pellegrinia, *Phys. Chem. Chem. Phys.*, 2013, **15**, 80-89.

28 C. Chung, Y. K. Kim, D. Shin, S. R. Ryoo, B. H. Hong, and D. H. Min, *Acc. Chem. Res.,* 2013, **46**, 2211-2224.

29 B. F. Machado and P. Serp*,Catal. Sci. Technol.,* 2012, **2**, 54-75.

30 Y. Wang, L. Polavarapu, and L. M. L. Marzán, *ACS Appl. Mater. Interfaces,* 2014, **6 (24),** 21798-21805.

31 J. Huang, L. Zhang, B. Chen, N. Ji, F. Chen, Y. Zhanga and Z. Zhang, *Nanoscale*, 2010, **2**, 2733-2738.

32 X. Chen, B. Jia, Y. Zhang and M. Gu, *Light: Science & Applications*, 2013, **2**, e92; doi:10.1038/lsa.2013.48

33 E. Stratakis, M. M. Stylianakis, E. Koudoumas and E. Kymakis, *Nanoscale*, 2013, **5**, 4144-4150.

34 Y. Xua, J. Luob, W. Yaob, J. Xub and T. Lia, *J. Alloy. Compd* , 2015, **636**, 310-316.

35 P. A. Cristobal, P. Vilela, A. E.Sagheer, E. L.Cabarcos, T. Brown, O. L. Muskens, J. R. Retama and A. G. Kanaras, *ACS Appl. Mater. Interfaces*, 2015, **7**, 12422-12429.

36 Y. Mao, S. Wen, Y. Chen, F. Zhang, P. Panine, T.W. Chan, L. Zhang, Y. Liang and L. Liu, *Sci. Rep.*, 2013, **3**, 2508. DOI:10.1038/srep02508 (2013).

37 T. S. Sreeprasad, S. M. Maliyekkal, K. P. Lisha, T. Pradeep, *J. Hazard. Mater.*, 2011, **186,** 921-931.

38 R. Muszynski, B. Seger and P. V. Kamat, *J. Phys. Chem. C*, 2008, **112 (14),** 5263-5266.

39 A. H. Jungemann, L. Kiessling, E. Stratakis, E. Kymakis, A. H. E. Sagheer, T. Brown and A. G. Kanaras, *J. Mater. Chem. C*, 2015, **3**, 9379-9384.

40 S. Badhulika, T. Terse-Thakoor, C. Villarreal, and A. Mulchandani, *Front Chem.,* 2015, **3,** 38.

41 W. S. Hummers, R. E. Offeman, *J. Am. Chem. Soc*., 1958, **80 (6)**, 1339.

42 D. C. Marcano, D. V. Kosynkin, J. M. Berlin, A. Sinitskii, Z. Sun, A. Slesarev, L. B. Alemany, W. Lu and J. M. Tour, *ACS Nano,* 2010, **4**, 4806-14.

43 K. Dave, K. H. Park and M. Dhayal, *RSC Advance*, 2015**, 5**, 95657-95665.

44 S. Stankovich, D. A. Dikin, R. D. Piner, K. A. Kohlhaas, A. Kleinhammes, Y. Jia, Y. Wu, S. T. Nguyen and R.S. Ruoff, *Carbon,* 2007, **45,** 1558−1565.

45 A. C. Ferrari and J. Robertson. *Physical Review B*., 2000, **61(20)**, 14095-140107.

46 W. Gao, L. B. Alemany, L. Ci and P. M. Ajayan, *Nat. Chem.* 2009, **1**, 403.

47 D. Yang, A. Velamakanni, G. Bozoklu, S. J. Park, M. Stoller, R. D. Piner, S. Stankovich, I. H. Jung, D. A. Field, C. A. J. Ventrice and R.S. Ruoff, *Carbon,* 2009, **47**, 145-152.

48 P. K. Chu and L. Li, *Materials Chemistry and Physics*, 2006, **96**, 253-277.

49 J. Jun, J. H. Shin and M. Dhayal, *App. Surf. Sci.*, 2006, **252(10)**, 3871-3877.

50 Y. S. Yuji, Y. Iijima, D. Asakawa and K. Hiraoka, *Surf. Interface Anal.,* 2010, **42(6-7)**, 658-661.

51 J. F. Moulder, W. F. Stickle, P. E. Sobol, and K. Bomben (J. Chastain, editor). Handbook of X-ray Photoelectron Spectroscopy. Perkin-Elmer Corporation (Physical Electronics) 1992.

52. H. Wanga and Y. H. Hu, *Energy Environ. Sci*., 2012, **5**, 8182-8188.

Figure Captions

Figure 1: Schematic representation of the steps involved for synthesis of hrGO-AuNP composite material by ultra-sonication. Optical image of colloidal suspension was obtained at each step and shown in the figure.

Figure 2: UV-vis spectra of **GO**, **hrGO** and **hrGO-AuNP**.

Figure 3: Raman spectra of graphite, **GO**, **hrGO** and **hrGO-AuNP**.

Figure 4: XRD pattern of (a) **GO**, (b) **hrGO** and (c) **hrGO-AuNP**.

Figure 5: TEM image of **hrGO-AuNP** (A) large view and (B) high resolution image. Arrow in the image (B) indicates folding of reduced graphene oxide sheets in **hrGO-AuNP**.

Figure 6: Wide scan XPS spectra of (a) **GO**, (b) **hrGO** and (c) **hrGO-AuNP**.

Figure 7: Peak fitted **C1s XPS spectra of (A) GO,** (B) **hrGO** and (C) **hrGO-AuNP**.

Figure 8: IV response of **GO** (black square), **hrGO** (red square) and **hrGO-AuNP** (green square).

Table Caption:

Table 1: Relative variation of different functionalities in **GO**, **hrGO** and **hrGO-AuNP**.

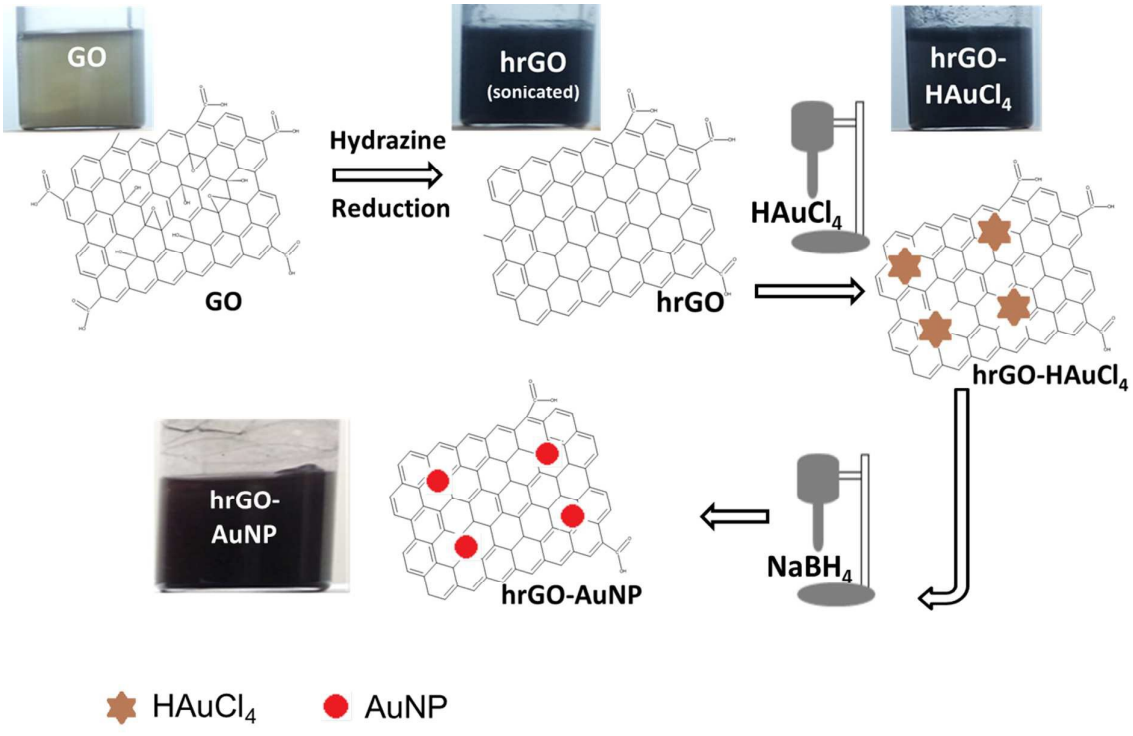

Figure 1: Schematic representation of the steps involved for synthesis of hrGO-AuNP composite material by ultra-sonication. Optical image of colloidal suspension was obtained at each step and shown in the figure.

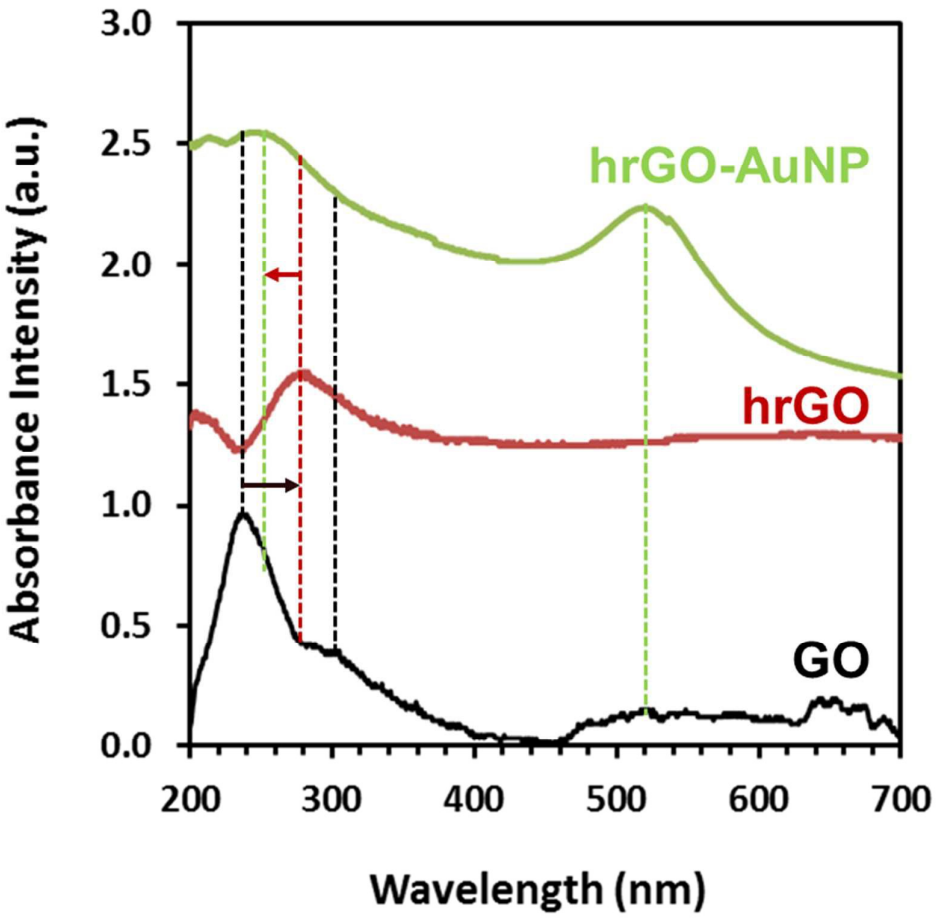

Figure 2: UV-vis spectra of **GO**, **hrGO** and **hrGO-AuNP**.

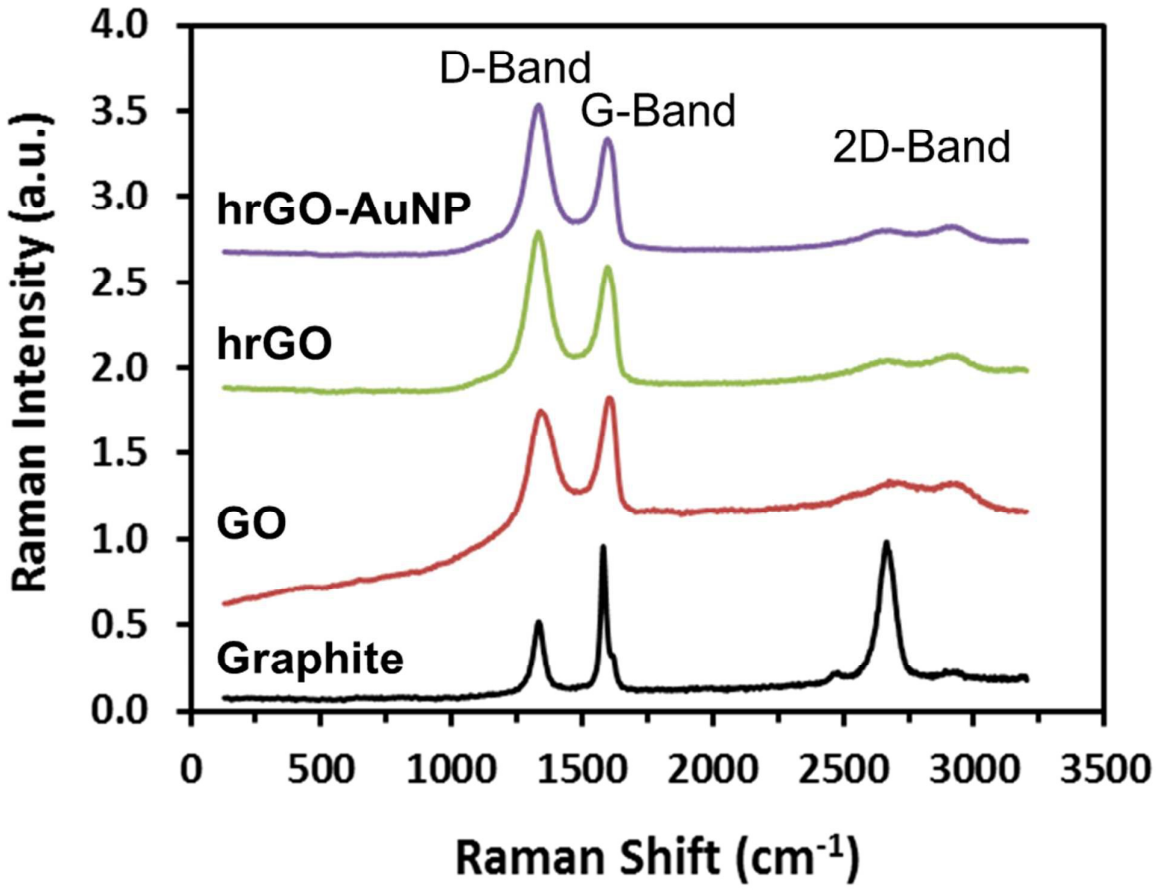

Figure 3: Raman spectra of graphite, **GO**, **hrGO** and **hrGO-AuNP**.

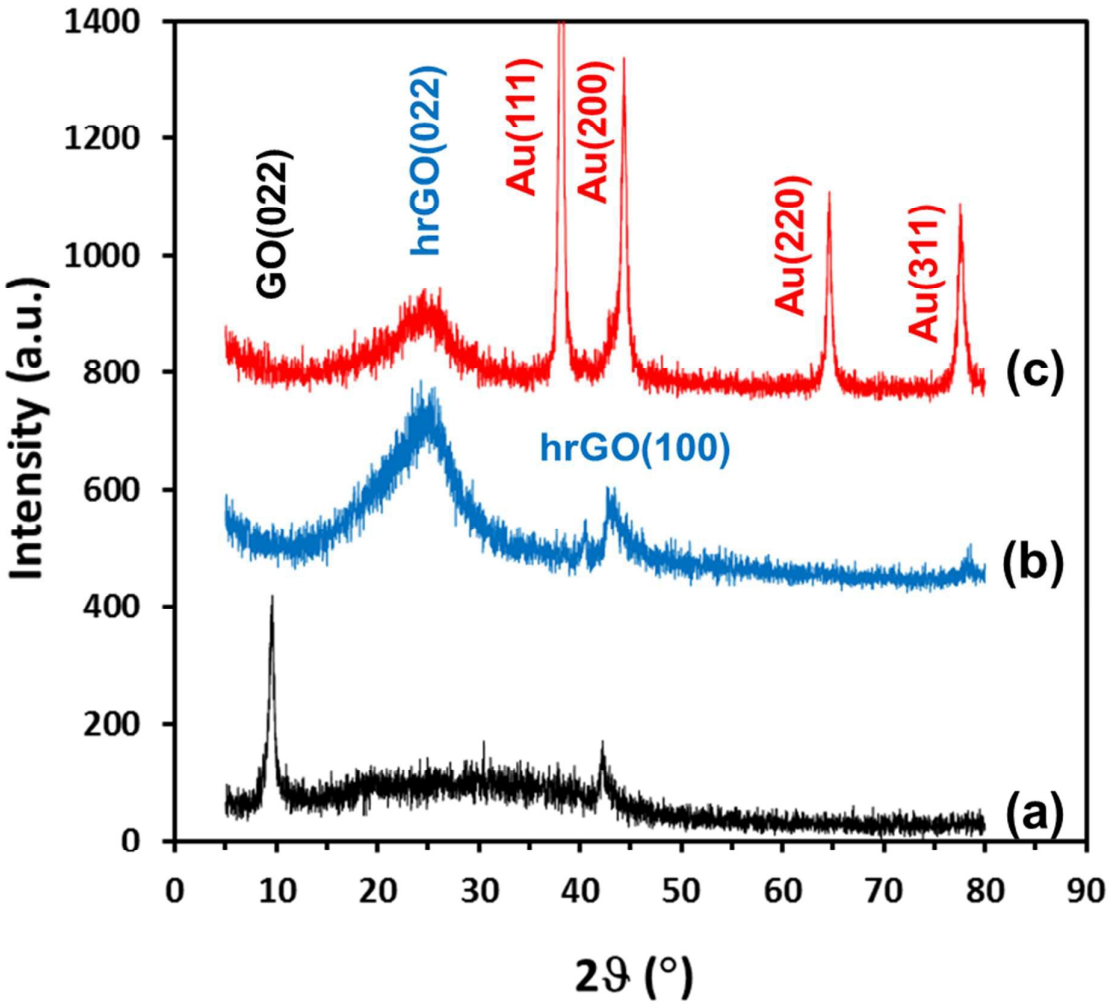

Figure 4: XRD pattern of (a) **GO**, (b) **hrGO** and (c) **hrGO-AuNP**.

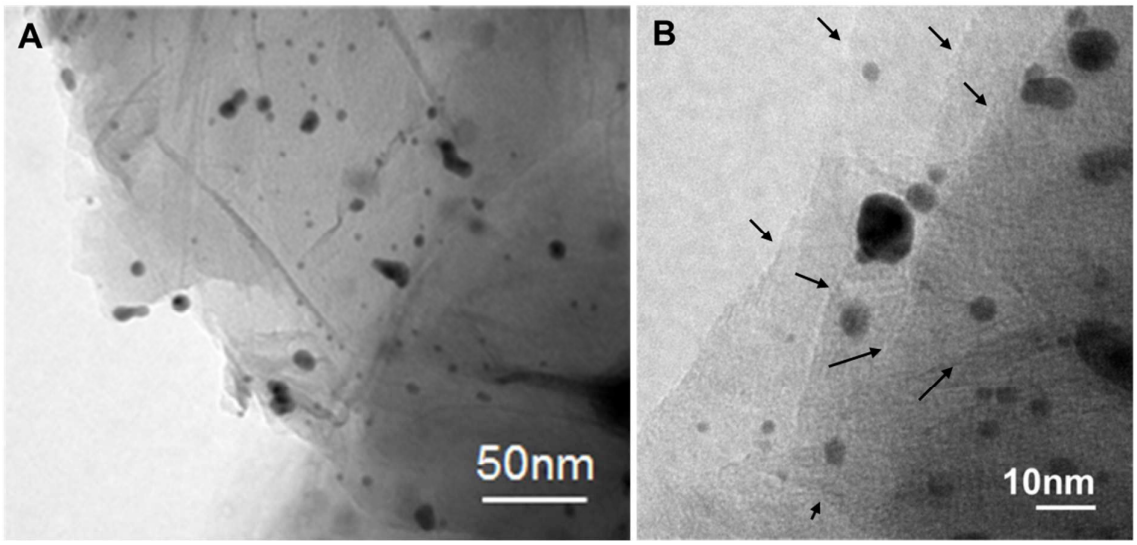

Figure 5: TEM image of **hrGO-AuNP** (A) large view and (B) high resolution image. Arrow in the image (B) indicates folding of reduced graphene oxide sheets in **hrGO-AuNP**.

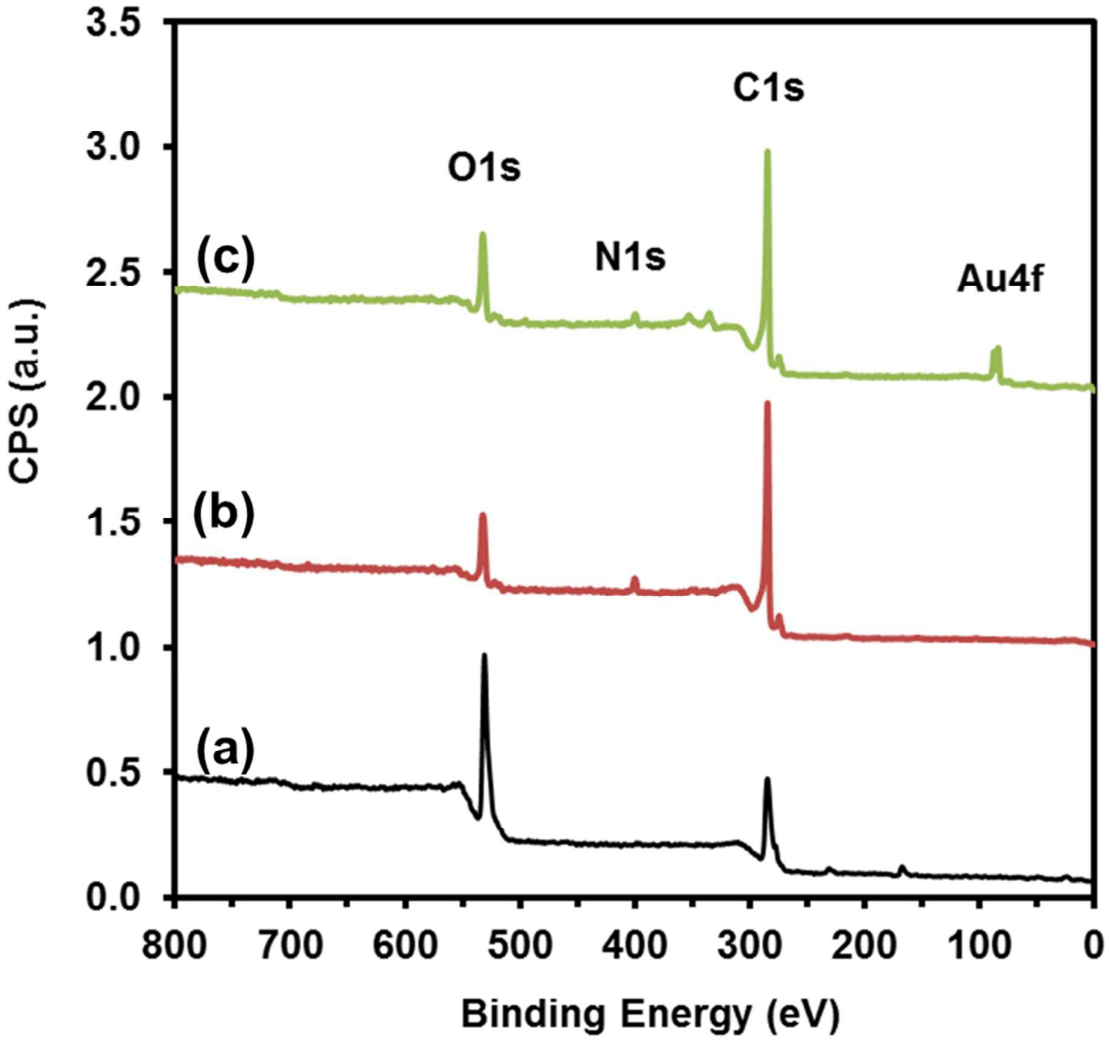

Figure 6: Wide scan XPS spectra of (a) **GO**, (b) **hrGO** and (c) **hrGO-AuNP**.

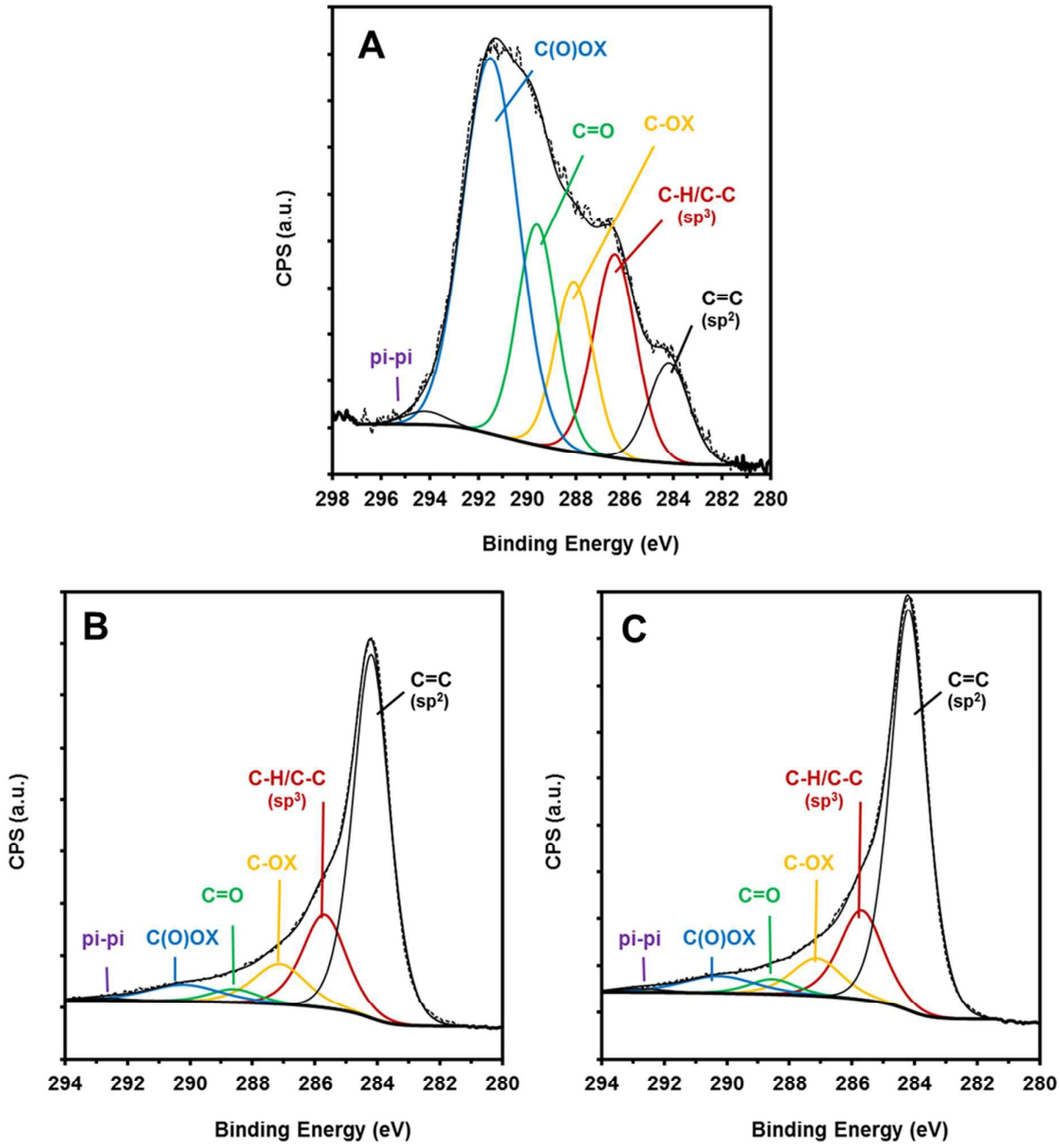

Figure 7: Peak fitted **C1s XPS spectra of (A) GO,** (B) **hrGO** and (C) **hrGO-AuNP**.

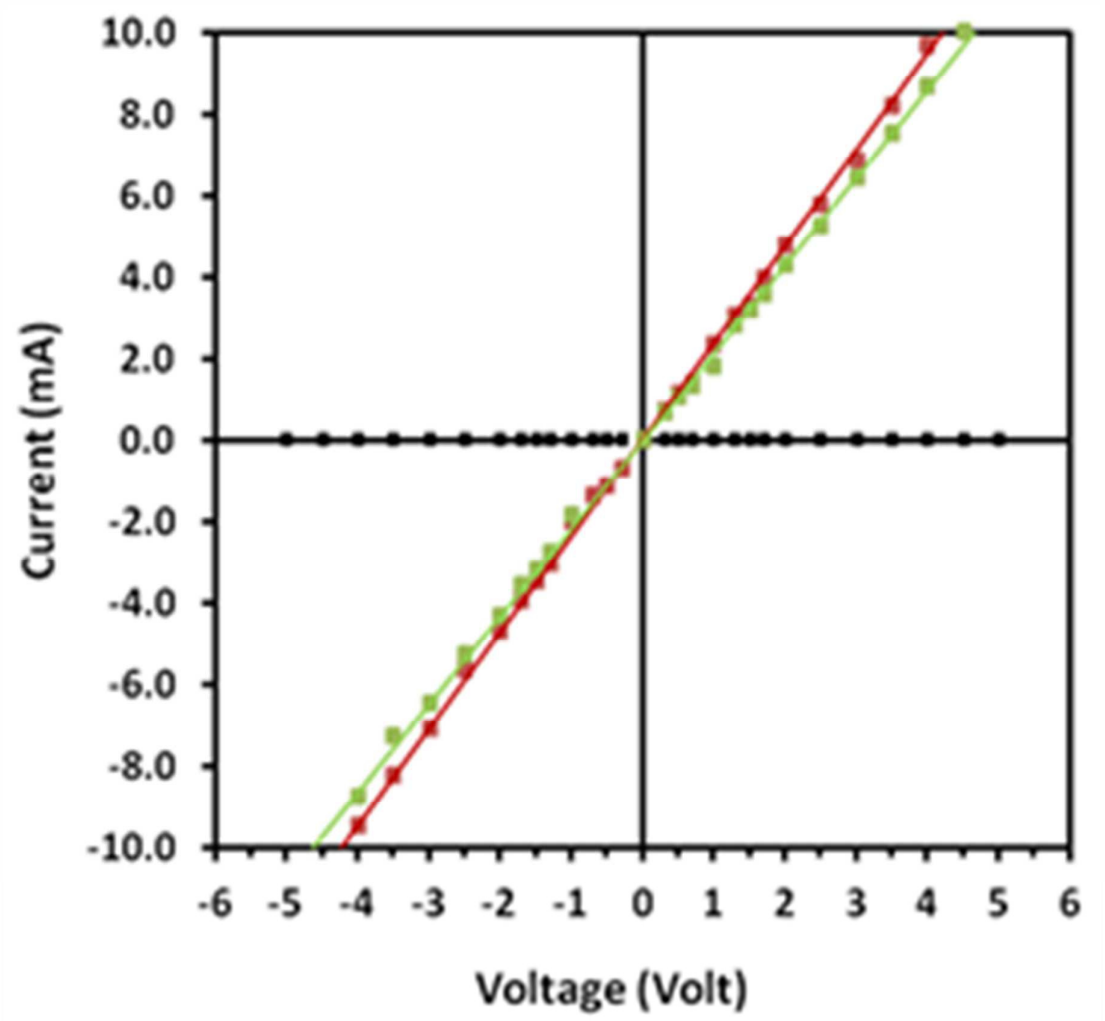

Figure 8: IV response of **GO** (black square), **hrGO** (red square) and **hrGO-AuNP** (green square).

Table 1: Relative variation of different functionalities in **GO**, **hrGO** and **hrGO-AuNP**.

Carbon / at %	GO	hrGO	hrGO-AuNP
$C(sp^2)$	8.3	64.8	56.4
$C(sp^3)$	17.7	17.2	26.9
C -OX	13.2	8.4	11.1
C =O	17.6	3.2	1.9
C (=O)OX	42.1	5.6	3.7
pi-pi	1.1	0.8	0

Graphical Abstract

Characteristics of Ultrasonication Assisted Assembly of Gold Nanoparticles in Hydrazine Reduced Graphene Oxide

Kashyap Dave[a], Kyung Hee Park[b], Marshal Dhayal[a†]

[a]Clinical Research Facility, CSIR-Centre for Cellular and Molecular Biology, Hyderabad 500007, India.

[b]Department of Dental Materials and Medical Research Center for Biomineralization Disorders, School of Dentistry, Chonnam National University, Gwangju 61186, Korea.

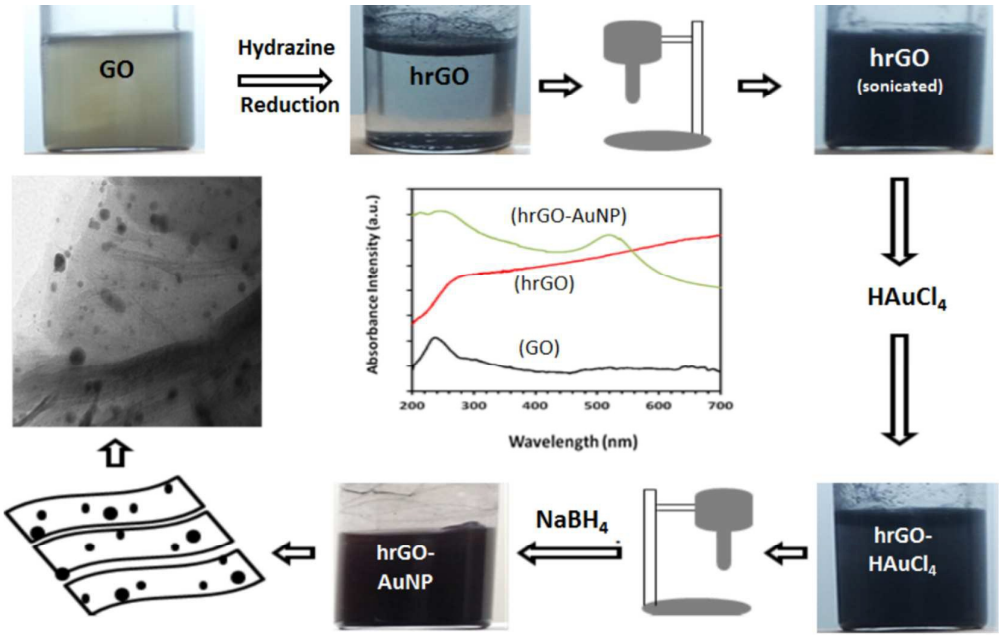

Graphene gold composites were synthesized by ultrasonication assisted *in-situ* reduction of diffused gold chloride within the hydrazine reduced graphene oxide sheets without surface modification or functionalization with organic molecules.